Breast Cancer Classification from Histopathological Images using Future Search Optimization Algorithm and Deep Learning

Ramalingam Gurumoorthy

Department of Computer and Information Science, Annamalai University, India
saragopi76@gmail.com (corresponding author)

Mari Kamarasan

Department of Computer and Information Science, Annamalai University, India
smkrasan@yahoo.com

ABSTRACT

In medical imaging, precise recognition of Breast Cancer (BC) is a challenge due to the complications of breast tissues. Histopathological detection is still considered the standard in BC detection. Still, the dramatic increase in workload and the complexity of histopathological image (HPI) make this task labor-intensive and dependent on the pathologist, making the advance of automated and precise HPI analysis techniques needed. Due to the automated feature extraction capability, Deep Learning (DL) methods have been effectively used in different sectors, particularly in the medical imaging sector. This study develops the future search algorithm with a DL-based breast cancer detection and classification (FSADL-BCDC) method. The FSADL-BCDC technique examines HPIs to detect and classify BC. To achieve this, the FSADL-BCDC technique implements Wiener Filtering (WF)-based preprocessing to eliminate the noise in the images. Additionally, the FSADL-BCDC uses the ResNeXt method for feature extraction with a Future Search Algorithm (FSA)-based tuning procedure. For BCDC, the FSADL-BCDC technique employs a Hybrid Convolutional Neural Network along with the Long Short-Term Memory (HCNN-LSTM) approach. Finally, the Sunflower Optimization (SFO) approach adjusts the hyperparameter values of the HCNN-LSTM. The outcomes of the FSADL-BCDC are inspected on a standard medical image dataset. Extensive relational studies highlighted the improved performance of the FSADL-BCDC approach in comparison with known methods by exhibiting an output of 96.94% and 98.69% under diverse datasets.

Keywords-deep learning; breast cancer; future search algorithm; histopathological images; computer-aided diagnosis

I. INTRODUCTION

Amongst the many kinds of cancer, Breast Cancer (BC) is ranked second among women. Moreover, the death rate of BC is comparatively higher than that of other cancer types [1]. The analysis of Histopathological Images (HPIs) is the most frequently employed technique for the diagnosis of BC in healthcare. In HPI analysis, the most significant task is classification [2]. The precise and automatic classification of high-resolution HPIs is the bottleneck and cornerstone of other in-depth studies like gland segmentation, nuclei localization, and mitosis detection [3]. Presently, histopathological imaging in medical practice mostly depends on manual analysis. But, at least three issues arise from this approach. At first, the possible lack of pathologists, especially in small hospitals and less developed areas [4]. This unbalanced distribution and resource shortage becomes a critical issue to be solved. Secondly, whether the histopathologic diagnosis is incorrect or correct relies on the long-term gathered diagnostic experience and professional knowledge of the given individual pathologist. This subjectivity has caused the growth of diagnostic inconsistencies [5]. Finally, the difficulty of the task makes pathologists liable to inattention and fatigue and so, keener to mistakes. Due to the similarity in features and irregular appearance between malignant and benign lesions, manual diagnosis is imprecise and difficult. To sort out such problems, it is vital to be precise and develop automatic HPI analytical approaches, namely classifier approaches. Computer-assisted diagnostic methods extract features from the nuclei to offer significant data to diagnose a lesion, either malignant or benign [6]. There are various clustering techniques and statistical approaches to extract features, classify, or segment nuclei [7]. In medical image diagnosis, there are several rapidly evolving techniques to classify HPIs, but there is still the need for more effective diagnosis. Complicated image-processing phases such as feature extraction, preprocessing, and segmentation are a

reason for low diagnostic accuracy. Hence, to sort out the Machine Learning (ML) problem, Deep Learning (DL) is presented to abstract the related attributes of the input raw images and utilize them for classification with more precision [8]. In DL, features are extracted through convolutional layers and assembly layers denoting more precision [9]. Currently, Convolutional Neural Networks (CNNs) are utilized to classify biomedical images. CNN works very well with huge datasets and is less precise on small datasets [10]. In small datasets, pre-trained CNNs are usually utilized.

This study introduces an innovative approach termed as Future Search Algorithm with DL-based Breast Cancer Detection and Classification (FSADL-BCDC). This technique incorporates several components to enhance its performance. At first, the FSADL-BCDC method employs Wiener Filtering (WF) as a pre-processing procedure for effective noise removal. Additionally, it leverages the ResNeXt model for feature extraction, optimizing hyperparameters using the FSA technique. For BCDC, the FSADL-BCDC method utilizes a Gybrid CNN with the Long Short-Term Memory (HCNN-LSTM) approach. To further fine-tune the HCNN-LSTM approach, the Sunflower Optimization (SFO) technique is employed for adjusting the hyperparameter values. The efficiency of the FSADL-BCDC technique is validated through experiments conducted on a well-established benchmark medical image dataset.

II. RELATED WORK

This section presents a short overview of recently developed BC classification models on HPIs. Authors in [11] developed a new CNN structure for classifying malignant and benign BC HPIs. Authors in [12] developed the AOADL-HBCC approach for making decisions. This approach uses noise removal depending on a contrast enhancement process and median filtering. Authors in [13] devised a BC-HPI classification that depends on deep FE-BkCapsNet to make full use of CapsNet and CNNs. Authors in [14] developed an automatic technique for diagnosing BC from HPIs. In this method, a residual learning-related 152-layered CNN termed ResHist was devised for classification. Authors in [15] applied ShuffleNet, Deep Neural Networks (DNNs), InceptionV3, and ResNet18 for the binary classification of BC in HPIs. They utilized pre-trained networks on the ImageNet dataset with layers given training on HPIs from BreakHis. In [16], a new technique depending on the Convolution-LSTM (CLSTM), with utilizing the Marker-controlled Watershed Segmentation Algorithm (MWSA) for preprocessing and SVM detection, was proposed. Authors in [17] focused on BC HPIs attained taking the assistance of the microscopic scan of breast tissues. The model joined two DCNNs to derive differentiated image aspects by employing TL. Authors in [18] introduced a frequency domain learning technique that relies on CNN and DWT for the classification task of BC HPIs. In [19], an enhanced model, IBESSDL-BCHI, was introduced for BC recognition by employing HPIs. The approach incorporates MF, Synergic DL (SDL), and LSTM techniques for preprocessing, tuning, and classification. Authors in [20] proposed the innovative HRLCE approach with two processing stages. Their method, the SAE-PSO-DNN model, combines

Particle Swarm Optimization (PSO) and Stacked Autoencoders (SAE) within a DNN framework.

III. THE PROPOSED MODEL

This article focuses on the design and development of the FSADL-BCDC approach for detecting and classifying BC. The main intention of the FSADL-BCDC method is to investigate HPIs in order to detect and classify BC. In the FSADL-BCDC method, the majorly involved procedures are WF-based preprocessing, ResNeXt feature extractor, FSA-based tuning, HCNN-LSTM classification, and SFO-based optimization. Figure 1 depicts the complete procedure of the FSADL-BCDC method.
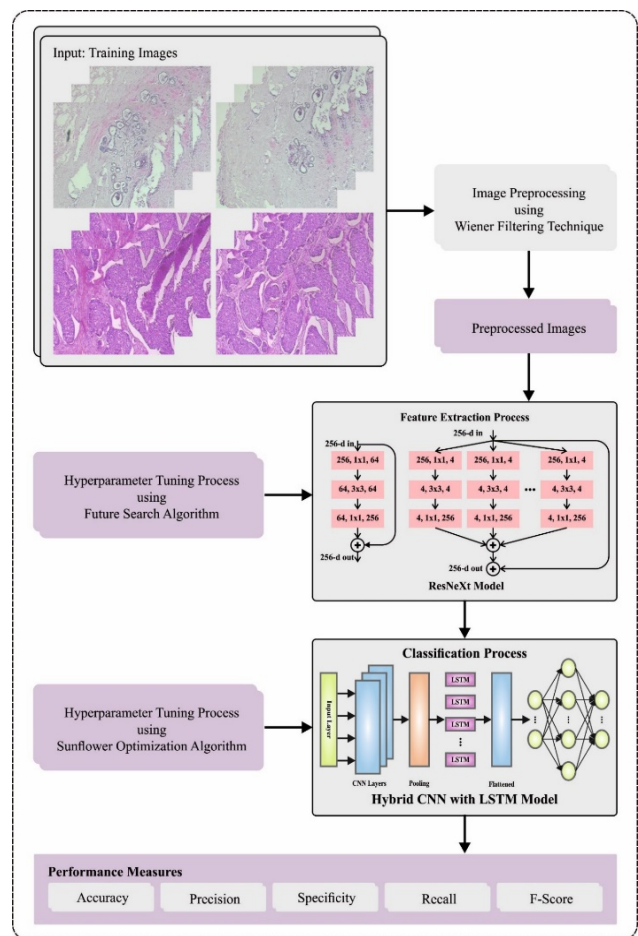
Fig. 1.   The overall process of the FSADL-BCDC approach.

A. Pre-processing

To eliminate noise from the input image, the WF technique is employed, functioning in the frequency domain of the image. The WF computes the Fourier transform of the image and the power spectrum of the noise, using a filter to reduce noise across all frequency components while preserving essential image details. In image processing, the WF curtails the mean squared error amid the original and filtered images, with adjustable filter parameters influencing performance, contingent on the accuracy of the assessed power spectrum of

the noise. Its efficacy in signal processing lies in minimizing mean square error, offering optimal linear estimation amidst noise, and its adaptability to diverse signal and noise characteristics renders it advantageous in specific applications.

B. Feature Extraction

ResNeXt method, an enhanced version of ResNet, is used for the extracting process. The parallel stacking block with a similar topology was utilized instead of the 3-layer convolution block [21]. The ResNeXt network consists of 4 ResNeXt block structures, namely 1 convolutional layer, 1 FC layer, 2 pooling layers, and 1 softmax classifier. Deep residual networking had cardinality and was composed of ResNeXt blocks. The leftover block can be changed by the split-transform-merge approach that results in branch routes within a cell. By the path of the skip connection, the output can be defined as:

$$OP = a + \sum_{i=1}^{ca} \tau_i (a) \qquad (1)$$

where τ_i, ca, OP, and a denote the arbitrary conversion, cardinality, and the earlier layer's output and input.

Every ResNeXt block has 3 convolutional layers and a shortcut connection. The 3 dissimilar kinds of convolution layers are convolution, group convolution, and convolution in series. Except for the final convolution layer, ReLU function is used to improve the network's non-linearity after the convolution layer. The ResNeXt block's group convolution stride is 2. Maxpooling is used to achieve spatial invariance and accelerate training while maintaining accuracy. The essential idea behind max -pooling was selecting the discriminatory features and representing a bunch of features.

$$v_{i,L}^{x,y} = \max_{m\in[0,m_i-1],n\in[0,n_i-1]}(x + m), (y + n) (i - 1), L (2)$$

where, m_i, n_i denote the size of kernels, and L is the index of the mapping features at the $(i—l)^{th}$ convolutional layer. The softmax classifier is utilized to implement the last classification. The early layers of the ResNeXt models capture simple features like edges, corners, and color gradients. The intermediate layers learn more complex features like shapes, textures, and object parts. The deeper layers can represent high-level semantic concepts and objects specific to the classes present in the ImageNet dataset.

C. Hyperparameter Tuning

In this work, the FSA optimizes the hyperparameter values in the ResNeXt approach by simulating optimal lifestyles for individuals, mapping this concept to the selection process of ResNeXt's hyperparameters. Employing a mathematical formula, the FSA enhances the initial random parameters through a global search among successful individuals and a local search within the population [22]. The FSA can be generated dependent upon mathematical formulas and begins phases depending on random solutions:

$$S(i,:) = Lb + (Ub - Lb) \times \text{rand}(1, d) \qquad (3)$$

where $S(i,:)$ denotes the ith solution, Lb and Ub signify the lower and upper boundaries, and rand implies the uniform distribution of a d-dimensional pseudorandom number.

Every solution is realized as the local (LS) and global (GS), solutions. Afterwards, this technique begins its iterations for determining the optimum solution. Primary, the search procedure in FSA is dependent upon the LS to assist the characteristics of exploitation.

$$S(i,:)_L = (LS(i,:) - S(i,:)) \times \text{rand} \qquad (4)$$

The search procedure of FSA in the search scope is dependent upon GS assisting the exploitation feature:

$$S(i,:)_G = (GS - S(i,:)) \times \text{rand} \qquad (5)$$

After estimating the local and global convergence, all the solutions are upgraded as:

$$S(i,:) = S(i,:) + S(i,:)_L + S(i,:)_G \qquad (6)$$

This technique upgrades GS and LS, and every solution is upgraded as:

$$S(i,:) = GS + (GS - S(i,:)) \times \text{rand} \qquad (7)$$

Lastly, the FSA will check the GS and LS and will update them if there are better solutions. The iterative procedure of FSA is projected as follows:

- Step 1. Arbitrarily determine the primary size of population, the main function, and its searching space. Fix the maximal iteration count Max. Set $t = 1$. Define the upper and lower limitations. Compute the primary GS and the primary LS. Initialize by (3).

- Step 2. The search process is dependent on LS in (4) and the global search is dependent on GS in (5). Calculate the local and global convergences. The outcome is determined in (6).

- Step 3. Relate the Fitness Function (FF) values of every possible solution to determine the GS and LS from the present generation. Compare the present GS and LS with the preceding values and upgrade if necessary. Upgrade the arbitrary primary (7).

- Step 4. Compute $t = t + 1$. See if $t =$ Max. If no, then go to Step 2. Else, stop and provide the resulting outcome.

D. Image Classification: The Optimal HCNN-LSTM Model

Finally, BC classification takes place using the HCNN-LSTM approach. The LSTM mostly overcomes the problems of gradient vanishing as a Recurrent Neural Network (RNN) variant, making the network more reliable and remembering the content for a long period. LSTM can be capable of removing or maximizing data [23]. LSTM consists of output, input, and forget gates, which are used for providing reset, read, and write functions. d_{t-1} shows the prior output of the model, X_t indicates the existing input used for producing novel memory, C_{t-1} denotes the prior cell state from the model, and the output data encompass the cell state C_t and the newest output d_t. A large amount of data will be flooding the memory once the input gate is opened. So, a forget gate is added for removing these data. Given X_t (existing input) and d_{t-1} (prior output), a number between 0 and 1 is acquired for all the digits at the cell state C_{t-1} (prior state), where 0 signifies completely discarded, and 1 indicates completely reserved:

$$F_t = \text{Sigmoid}\big(W_f[d_{t-1}, x_t] + b_f\big) \tag{8}$$

In (8), b_f indicates the bias term, W_f shows the weight matrix, and the resultant value through this networking lies inside [0, 1], which shows that the prior cell state probability has been forgotten, 1 is "fully saved" and 0 is "completely deleted".

After circulating NN's forget part of the prior state, the LSTM's input gate needs to add the new memory from the present input. This procedure should be satisfied by the input gate, which includes two segments, namely a sigmoid layer that defines which value must be renewed and a tanh layer that decides a new candidate vector $\widetilde{C}_t$ increased to this state:

$$h_t = \sigma(W_n \cdot [d_{t-1}, X_t] + bn) \tag{9}$$

$$\tilde{C}_t = \tanh(W_M \cdot [d_{t-1}, X_t] + bm) \tag{10}$$

$$C_t = F_t \times C_{t-1} + h_t \times \tilde{C}_t \tag{11}$$

where W_n, b_m, h_t, C_t, and W_M portray the weighted matrix, the bias item to update state, the input gate, the upgraded memory unit state, and the weighted matrix to upgrade the layer. C_t takes the dot product of the forget gate F_t with C_{t-1} for determining if it remembers its value, h_t and $\widetilde{C}_t$ determine whether to upgrade C_t, and b_n symbolizes the biased item. The output gate decides the present, the newest, and the final output. The LSTM's resulting gate is the outcome of the present moment that should be produced after evaluating the newest state:

$$d_r = 0_t \times \tanh(C_t) \tag{12}$$

$$0_t = \sigma(WV_O[d_{t-1}, x_t] + b_O) \tag{13}$$

where d_t is correlated to C_t and to the input x_t at the t time step and the hidden layer's value of activation d_{t-1} at the prior time-step. The sigmoid function is used to attain O_t within [0,1], and later multiplies C_t with O_t and tanh. The CNN and LSTM, conventional in DL models, excel in spatial abstraction/local feature extraction and sequential/temporal processing, respectively. Recent studies manage enhanced stability by merging both methods, leading this study to adopt a parallel connection for a CNN–LSTM architecture, emphasizing the interconnected features of CNN and LSTM networks [23]. Leveraging the SFO method, adjustments to hyperparameter values in the HCNN-LSTM approach mimic the daily sunflower cycle, offering an effective strategy for hyperparameter tuning in the CNN-LSTM model [24]. The amount of heat Q_i obtained by all the plants can be defined as:

$$Q_i = \frac{P}{4\pi r_i^2} \tag{14}$$

where P, r_i denote the source of power and the distance among them. The sunflower faces the sun in the succeeding path:

$$\vec{S}_i = \frac{X^* - X_i}{||X^* - X_i||}, \text{ where } i = 1,2,3,\ldots,n \tag{15}$$

The sunflower direction is evaluated as:

$$d_i = \alpha \times Pi(Xi + Xi - 1) \times ||Xi + Xi - 1|| \tag{16}$$

In (16), the possibility of pollination is $Pi(||Xi + Xi - 1|$ that implies the sunflower i will be pollinating its adjacent neighbor $i - l$ and generate a new one in an arbitrary location, whereas α denotes the inertial displacement. The maximal step can be formulated as:

$$d_{\max} = \frac{||X_{\max} - X_{\min}||}{2 \times N_{pop}} \tag{17}$$

In (17), $X_{\max}$ and $X_{\min}$ denote the maximum and minimum values. N_{pop} indicates the overall plant number in the population. The newest plantation can be defined by:

$$\overrightarrow{X_{i+1}} \to = \vec{x}_i + d_i \times \to \vec{s}_i \tag{18}$$

In the SFO approach, the selection of fitness relies on evaluating the candidate goodness using an encoder output, with accuracy being the pivotal criterion for defining the FF:

$$Fitness = \max\left(\frac{TP}{TP + FP}\right) \tag{19}$$

where TP and FP characterize the True and False Positive values.

IV. RESULTS AND DISCUSSION

In this section, the investigational output evaluation of the FSADL-BCDC approach is experimented on the BreakHis dataset [25]. The BreakHis dataset offers a distinctive advantage by providing a comprehensive collection of histopathological imaging. Its categorization into benign and malignant tumors across multiple magnifications enhances the dataset's suitability for diverse and specialized studies. It comprises the datasets 40X and 100X magnification, consisting of 1995 and 2081 samples, respectively. In Figure 2, the relational outputs of the FSADL-BCDC method with recent models [26] are portrayed on the 40X dataset. It can be seen that the FSADL-BCDC method portrayed increased $accu_y$, $prec_n$, and $reca_l$ of 96.94%, 96.71%, and 96.94%. It can be seen that PFTAS-QDA, ResNet50, Xception, Inception-v3, and Inception-ResNetv2 approaches reached lesser $accu_y$, $prec_n$, and $reca_l$ values.
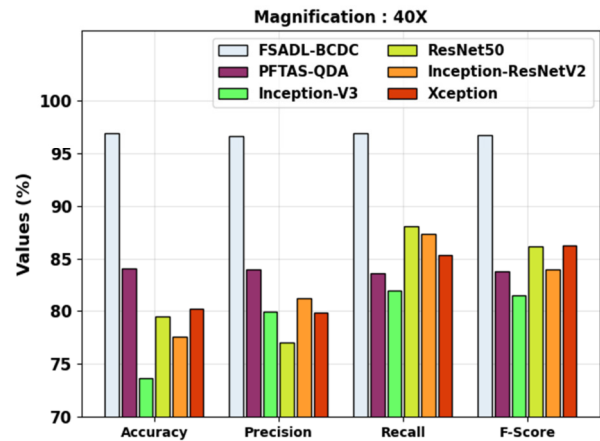
Fig. 2.   Comparative analysis of the FSADL-BCDC approach on the 40X dataset.
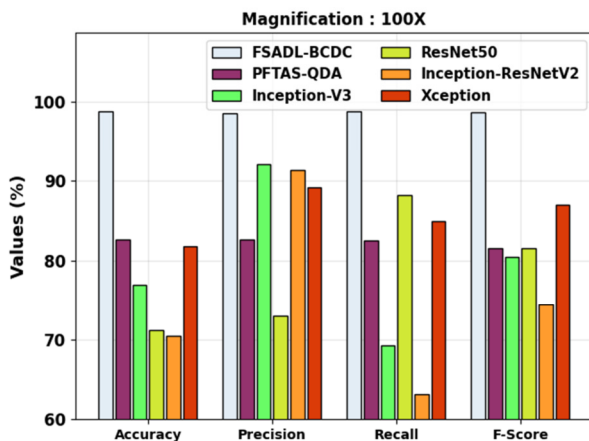
Fig. 3.   Comparative analysis of the FSADL-BCDC approach on the 100X dataset.

In Figure 3, the relative output of the FSADL-BCDC approach is given on the 100X dataset. It can be seen that the FSADL-BCDC approach offers increased $accu_y, prec_n, reca_l$ of 98.69%, 98.47%, and 98.69%, whereas the PFTAS-QDA, ResNet50, Xception, Inception-v3, and Inception-ResNetv2 approaches attained lesser $accu_y, prec_n$, and $reca_l$ values.

V.   CONCLUSION

In this article, focus is given on the design and development of the FSADL-BCDC methodology for detecting and classifying BC from HPIs. The main objective of the FSADL-BCDC methodology is to investigate HPIs to detect and classify BC. In the FSADL-BCDC technique, the involved processes are WF-based preprocessing, ResNeXt feature extractor, FSA-based tuning, HCNN-LSTM classification, and SFO-based optimization. The utilization of the FSA and SFO techniques enhances the detection and classification performance of the FSADL-BCDC technique. The investigational outputs of the FSADL-BCDC method are examined on a standard medical image dataset. Extensive comparison studies highlighted the achievement of 96.94% and 98.69% enhanced accuracy of the proposed method under diverse data, which surpasses the considered existing techniques. Thus, the FSADL-BCDC method can be utilized for the automated classification of BC. In the future, the performance of the FSADL-BCDC method can be enhanced by the design of ensemble classifier methods. The FSADL-BCDC method may encounter challenges in handling diverse histopathological images and could be sensitive to variations in image quality. Also, the reliance on sunflower optimization for tuning may pose computational complexities and scalability issues in large-scale datasets.

REFERENCES

[1] Y. Wang *et al.*, "Breast Cancer Image Classification via Multi-Network Features and Dual-Network Orthogonal Low-Rank Learning," *IEEE Access*, vol. 8, pp. 27779–27792, Jan. 2020, https://doi.org/10.1109/ACCESS.2020.2964276.

[2] Y. Celik, M. Talo, O. Yildirim, M. Karabatak, and U. R. Acharya, "Automated invasive ductal carcinoma detection based using deep transfer learning with whole-slide images," *Pattern Recognition Letters*, vol. 133, pp. 232–239, May 2020, https://doi.org/10.1016/j.patrec.2020.03.011.

[3] I. Hirra *et al.*, "Breast Cancer Classification From Histopathological Images Using Patch-Based Deep Learning Modeling," *IEEE Access*, vol. 9, pp. 24273–24287, Feb. 2021, https://doi.org/10.1109/ACCESS.2021.3056516.

[4] S. Boumaraf, X. Liu, Z. Zheng, X. Ma, and C. Ferkous, "A new transfer learning based approach to magnification dependent and independent classification of breast cancer in histopathological images," *Biomedical Signal Processing and Control*, vol. 63, Jan. 2021, Art. no. 102192, https://doi.org/10.1016/j.bspc.2020.102192.

[5] S. Chattopadhyay, A. Dey, P. K. Singh, and R. Sarkar, "DRDA-Net: Dense residual dual-shuffle attention network for breast cancer classification using histopathological images," *Computers in Biology and Medicine*, vol. 145, Jun. 2022, Art. no. 105437, https://doi.org/10.1016/j.compbiomed.2022.105437.

[6] R. Gurumoorthy and M. Kamarasan, "Computer Aided Breast Cancer Detection and Classification using Optimal Deep Learning," in *2023 International Conference on Sustainable Computing and Data Communication Systems (ICSCDS)*, Mar. 2023, pp. 143–150, https://doi.org/10.1109/ICSCDS56580.2023.10105045.

[7] N. Venugopal, K. Mari, G. Manikandan, and K. R. Sekar, "Phase quantized polar transformative with cellular automaton for early glaucoma detection," *Ain Shams Engineering Journal*, vol. 12, no. 4, pp. 4145–4155, Dec. 2021, https://doi.org/10.1016/j.asej.2021.04.018.

[8] N. Liu, E.-S. Qi, M. Xu, B. Gao, and G.-Q. Liu, "A novel intelligent classification model for breast cancer diagnosis," *Information Processing & Management*, vol. 56, no. 3, pp. 609–623, May 2019, https://doi.org/10.1016/j.ipm.2018.10.014.

[9] S. M. Shaaban, M. Nawaz, Y. Said, and M. Barr, "An Efficient Breast Cancer Segmentation System based on Deep Learning Techniques," *Engineering, Technology & Applied Science Research*, vol. 13, no. 6, pp. 12415–12422, Dec. 2023, https://doi.org/10.48084/etasr.6518.

[10] K. Aldriwish, "A Deep Learning Approach for Malware and Software Piracy Threat Detection," *Engineering, Technology & Applied Science Research*, vol. 11, no. 6, pp. 7757–7762, Dec. 2021, https://doi.org/10.48084/etasr.4412.

[11] X. Li, X. Shen, Y. Zhou, X. Wang, and T.-Q. Li, "Classification of breast cancer histopathological images using interleaved DenseNet with SENet (IDSNet)," *PLOS ONE*, vol. 15, no. 5, 2020, Art. no. e0232127, https://doi.org/10.1371/journal.pone.0232127.

[12] M. Obayya *et al.*, "Hyperparameter Optimizer with Deep Learning-Based Decision-Support Systems for Histopathological Breast Cancer Diagnosis," *Cancers*, vol. 15, no. 3, Jan. 2023, Art. no. 885, https://doi.org/10.3390/cancers15030885.

[13] P. Wang, J. Wang, Y. Li, P. Li, L. Li, and M. Jiang, "Automatic classification of breast cancer histopathological images based on deep feature fusion and enhanced routing," *Biomedical Signal Processing and Control*, vol. 65, Mar. 2021, Art. no. 102341, https://doi.org/10.1016/j.bspc.2020.102341.

[14] M. Gour, S. Jain, and T. Sunil Kumar, "Residual learning based CNN for breast cancer histopathological image classification," *International Journal of Imaging Systems and Technology*, vol. 30, no. 3, pp. 621–635, 2020, https://doi.org/10.1002/ima.22403.

[15] A. Aloyayri and A. Krzyżak, "Breast Cancer Classification from Histopathological Images Using Transfer Learning and Deep Neural Networks," in *Artificial Intelligence and Soft Computing*, 2020, pp. 491–502, https://doi.org/10.1007/978-3-030-61401-0_45.

[16] F. Demir, "DeepBreastNet: A novel and robust approach for automated breast cancer detection from histopathological images," *Biocybernetics and Biomedical Engineering*, vol. 41, no. 3, pp. 1123–1139, Jul. 2021, https://doi.org/10.1016/j.bbe.2021.07.004.

[17] H. Elmannai, M. Hamdi, and A. AlGarni, "Deep Learning Models Combining for Breast Cancer Histopathology Image Classification," *International Journal of Computational Intelligence Systems*, vol. 14, no. 1, pp. 1003–1013, Mar. 2021, https://doi.org/10.2991/ijcis.d.210301.002.

[18] Y. Qi, X. Liu, H. Li, M. Liu, and W. Li, "Discrete Wavelet Transform-Based CNN for Breast Cancer Classification from Histopathology Images," in *Machine Learning for Cyber Security*, 2023, pp. 326–340, https://doi.org/10.1007/978-3-031-20096-0_25.

[19] M. A. Hamza *et al.*, "Improved Bald Eagle Search Optimization with Synergic Deep Learning-Based Classification on Breast Cancer Imaging," *Cancers*, vol. 14, no. 24, Jan. 2022, Art. no. 6159, https://doi.org/10.3390/cancers14246159.

[20] K. Sangeetha and S. Prakash, "An Early Breast Cancer Detection System Using Stacked Auto Encoder Deep Neural Network with Particle Swarm Optimization Based Classification Method," *Journal of Medical Imaging and Health Informatics*, vol. 11, no. 12, pp. 2897–2906, Dec. 2021, https://doi.org/10.1166/jmihi.2021.3886.

[21] S. S. R. Bairaboina and S. R. Battula, "Ghost-ResNeXt: An Effective Deep Learning Based on Mature and Immature WBC Classification," *Applied Sciences*, vol. 13, no. 6, Jan. 2023, Art. no. 4054, https://doi.org/10.3390/app13064054.

[22] Y. Fan, S. Zhang, H. Yang, D. Xu, and Y. Wang, "An Improved Future Search Algorithm Based on the Sine Cosine Algorithm for Function Optimization Problems," *IEEE Access*, vol. 11, pp. 30171–30187, Mar. 2023, https://doi.org/10.1109/ACCESS.2023.3258970.

[23] X. Zhou, J. Feng, and Y. Li, "Non-intrusive load decomposition based on CNN–LSTM hybrid deep learning model," *Energy Reports*, vol. 7, pp. 5762–5771, Nov. 2021, https://doi.org/10.1016/j.egyr.2021.09.001.

[24] S. Al-Otaibi, V. Cherappa, T. Thangarajan, R. Shanmugam, P. Ananth, and S. Arulswamy, "Hybrid K-Medoids with Energy-Efficient Sunflower Optimization Algorithm for Wireless Sensor Networks," *Sustainability*, vol. 15, no. 7, Jan. 2023, Art. no. 5759, https://doi.org/10.3390/su15075759.

[25] F. Spanhol, L. S. Oliveira, C. Petitjean, and L. Heutte, "Breast Cancer Histopathological Database (BreakHis) - Laboratório Visão Robótica e Imagem." Jun. 20, 2017, [Online]. Available: https://web.inf.ufpr.br/vri/databases/breast-cancer-histopathological-database-breakhis/.

[26] M. Liu, Y. He, M. Wu, and C. Zeng, "Breast Histopathological Image Classification Method Based on Autoencoder and Siamese Framework," *Information*, vol. 13, no. 3, Mar. 2022, Art. no. 107, https://doi.org/10.3390/info13030107.